HHS Public Access

Author manuscript

Mol Pharm. Author manuscript; available in PMC 2022 June 30.

Published in final edited form as:

Mol Pharm. 2019 April 01; 16(4): 1766–1774. doi:10.1021/acs.molpharmaceut.9b00144.

Cyclodextrin polymer preserves sirolimus activity and local persistence for anti-fibrotic delivery over the time course of wound healing

Nathan A. Rohner[1], **Steve J. Schomisch**[2], **Jeffrey M. Marks**[3], **Horst A. von Recum**[*,1]

[1]Department of Biomedical Engineering, Case Western Reserve University, 10900 Euclid Ave., Cleveland, OH 44106

[2]Department of Surgery, Case Western Reserve University, 10900 Euclid Ave., Cleveland, OH 44106

[3]Department of Surgery, University Hospitals Cleveland Medical Center, 11100 Euclid Ave., Cleveland, OH 44106

Abstract

Fibrosis and dysphagic stricture of the esophagus is a major unaddressed problem often accompanying endoscopic removal of esophageal cancers and pre-cancerous lesions. While weekly injections of anti-proliferative agents show potential for improved healing, repeated injections are unlikely clinically, and may alternatively be replaced by creating an esophageal drug delivery system. Affinity-based polymers have previously shown success for continuous delivery of small molecules for weeks to months. Herein, we explored the potential of an affinity-based microparticle to provide long-term release of an anti-proliferative drug, sirolimus. In molecular docking simulations and surface plasmon resonance experiments sirolimus was found to have suitable affinity for beta-cyclodextrin while dextran, as a low affinity control, was validated. Polymerized beta-cyclodextrin microparticles exhibited 30 consecutive days of delivery of sirolimus during *in vitro* release studies. In total, the polymerized beta-cyclodextrin microparticles released 36.9 milligrams of sirolimus per milligram of polymer after one month of incubation *in vitro*. Taking daily drug release aliquots and applying them to PT-K75 porcine mucosal fibroblasts we observed that cyclodextrin microparticle delivery preserved bioactivity of sirolimus inhibiting proliferation by 27−67% and migration of fibroblasts by 28−100% of buffer treated controls *in vitro*. Testing for esophageal injection site losses, no significant loss was incurred under simulated saliva flow for 10 minutes, and 16.7% of fluorescently labeled polymerized cyclodextrin microparticle signal was retained at 28 days after submucosal injection in esophageal tissue *ex vivo* versus only 4% of the initial amount remaining for free dye molecules injected alone. By combining affinity-based drug delivery for continuous long-term

[*]Corresponding Author: Horst A. von Recum, 10900 Euclid Ave, Cleveland, OH 44106, Fax: (216) 368-5513; Tel: (216) 368-4969; horst.vonrecum@case.edu.

Disclosures

H.A. von Recum is a co-founder of Affinity Therapeutics but does not receive salary. J.M. Marks is a consultant for Olympus and Boston Scientific. The other authors have nothing to disclose.

Supporting Information. Images of porcine mucosal fibroblast scratch assay with SRL

release with a microparticle platform that is injectable yet remains localized in tissue interstitium, this combination platform demonstrates promise for preventing esophageal fibrosis and stricture.

Graphical Abstract

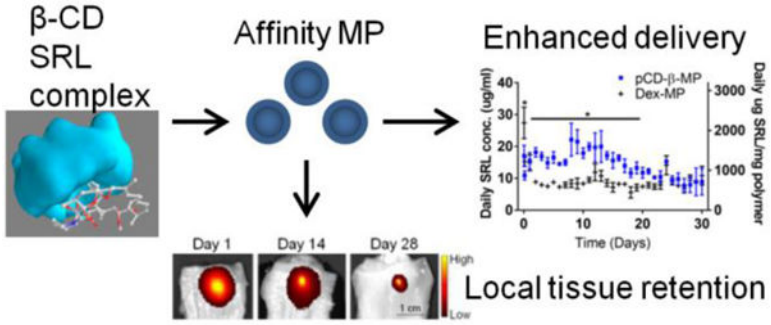

Keywords

Drug delivery; affinity; polymers; regenerative medicine; gastrointestinal wound healing; esophagus; stricture; inflammation

1. Introduction

Esophageal cancer is the 18th most common cancer in the United States with an estimated 17,290 new cases and 15,850 related deaths occurring in 2018 [1]. Improved survival outcomes correlate with early detection and early treatment. While critical changes in early detection methods are in development [2], minimally invasive early treatment options still exhibit some drawbacks [3–5]. Endoscopic submucosal dissection (ESD) is one such treatment option for early stage esophageal cancers and cases of Barrett's esophagus with high-grade dysplasia [6–7]. ESD is advantageous as complete removal of cancerous tissue can be confirmed via histology of en bloc resected tissue and the procedure has proven to increase disease-free survival rates [8–11]. However, fibrotic processes accompanying ESD often result in scarring and dysphagic stricture of the esophagus, especially in patients with extensive or circumferential ESD for which post-procedure stricture rates of 70% and higher have been reported [12–15]. Post-surgical attempts to relieve stricture, such as mechanical balloon dilation require many procedures due to the refractory nature of the stricture over months to years with risk of perforation, internal bleeding, and reduced patient quality of life. Other strategies include introducing a stent, applying surgical meshes, and steroid therapies, yet none have sufficiently addressed post-ESD stricture to improve patient quality of life [12, 16–19].

Interestingly, repeated local injections of anti-scarring agents to underlying tissue after ESD was observed to reduce esophageal stricture by up to 50% at four weeks post-ESD [20]. However, multiple, weekly intra-esophageal injections over the time course of wound healing present a clinical and patient burden similar to repeated esophageal balloon dilation procedures and risk perforation and abscess formation due to multiple injections. Additionally, high local concentrations of mitomycin C were observed to exhibit deleterious

effects [20]. A more tolerable agent, sirolimus (SRL; rapamycin), is explored in this study. SRL has indicated potential for anti-scarring therapy in glaucoma surgery and has been shown to reduce the rate of restenosis of coronary lesions [21–22]. However, SRL is a small molecule drug (MW=914.172 g/mol) with poor oral bioavailability and a limited tissue half-life of only 62 hours as compared to the four week timeline of wound healing [23–24]. Therefore, we explored the potential of using a drug delivery system to provide long-term, local release of SRL as an anti-fibrotic therapy.

In previous work, polymerized cyclodextrins (pCD) have demonstrated the ability to continuously deliver small molecule drugs on the order of weeks to months by leveraging affinity interactions [25–31]. Cyclodextrin monomers are polymerized into larger macrostructures such as disks and particles or even device coatings in order to achieve a high concentration of affinity binding sites to delay drug release [27, 32–36]. pCD-based materials are capable of loading high amounts of many classes of drugs while extending release for several months compared to low affinity interactions that typically release >95% of drug within a week, which is clinically insufficient for the timeline of wound healing expected in ESD [37]. Herein the potential of polymerized cyclodextrin microparticles (pCD-MP) to release SRL for an extended time, the efficacy of released SRL to regulate proliferation and migration, and the retention of pCD-MP in esophageal tissue *in vitro* under diffusion and flow conditions is evaluated.

2. Experimental Section

2.1 Materials

β-cyclodextrin (β-CD) prepolymer, lightly crosslinked with epichlorohydrin, and 6-deoxy-6-amino β-cyclodextrin heptahydrochloride and 6-deoxy-6-amino γ-cyclodextrin octohydrochloride were purchased from CycloLab (Budapest, Hungary). Ethylene glycol diglycidyl ether was purchased from Polysciences, Inc. (Warrington, PA). Dextran (15−25k molecular weight) was purchased from Sigma-Aldrich (St. Louis, MO). SRL (rapamycin) was purchased from Biotang (Lexington, MA). 3A-amino-3A-deoxy-alpha-cyclodextrin, amino-dextran, and all other reagents, solvents, and chemicals were purchased from Thermo Fisher Scientific (Hampton, NH) in the highest grade available.

2.2 Microparticle Synthesis

Epichlorohydrin-crosslinked β-cyclodextrin prepolymer (or dextran for non-affinity control) was solubilized in 0.2 M potassium hydroxide (25% w/v) and heated to 60°C for 10 minutes. Light mineral oil was warmed in a beaker with a Tween85/Span85 solution (24%/76%) and stirred at 500 RPM. Next, ethylene glycol diglycidyl ether was added drop-wise and the solution was vortexed for 2 minutes before pouring into the beaker with the oil/Span/Tween85 mixture, increasing the temperature to 70°C, and increasing the stir speed. The reaction was carried out for 3 hours to form polymerized cyclodextrin microparticles. The microparticles were then centrifuged at 200xg to be separated from the oil mixture, washed with excess hexanes twice, excess acetone twice, and finally de-ionized water (diH_2O) twice. The microparticles were resuspended, frozen, and lyophilized before further use.

2.3 Microparticle Characterization

Microparticles were resuspended (1 mg/ml) in Dulbecco's phosphate buffered saline (DPBS) with 0.1% Tween80 (polysorbate 80). Particles sizes were measured from images taken with a Nikon Eclipse TE300 inverted microscope (Nikon Inc., Tokyo, Japan) after 1 and 30 days of incubation.

2.4 Molecular Docking Simulations

Molecular structure data files for SRL and β-CD were downloaded from the PubChem database. Structures were converted to PDBQT format and energy was minimized before loading SRL as a ligand and cyclodextrins or dextran as a host in PyRx (Molecular Graphics Laboratory, The Scripps Research Institute, La Jolla, CA). The Autodock Vina algorithm was used to predict the strength of the ligand/guest interaction [38–39]

2.5 Surface Plasmon Resonance

The binding strength between a variation of cyclodextrin monomers and SRL was measured experimentally through surface plasmon resonance (SPR) with a Biacore X100 system (GE Healthcare Bio-Sciences, Pittsburgh, PA). Conditions used were based upon previous optimization for small molecule drugs binding to cyclodextrins [33, 36]. The surface of each sensor chip CM-3 was conjugated with EDC (0.4 M) and NHS (0.1 M) followed by either 10 mM 6-amino-6-deoxy-β-cyclodextrin (Cyclolab) or 6-deoxy-6-amino γ-cyclodextrin (CycloLab) or 3A-amino-3A-deoxy-alpha-cyclodextrin (ThermoFisher Scientific) suspended in HBS-N buffer (a HEPES balanced salt solution with pH 7.4). The other channel was conjugated similarly with amino-dextran (Thermo Fisher Scientific) to determine specific versus nonspecific interactions with a chemically similar but non-affinity substrate. The remaining functional groups were capped by running ethanolamine through both channels. A multi-cycle kinetic experiment was performed on each chip individually with SRL dissolved in a 1% dimethylsulfoxide MilliQ water solution. The surface was regenerated with 50 mM sodium hydroxide between samples to fully dissociate any remaining bound drug. The differential responses between the channels were fit to both steady state affinity and a 1:1 kinetics binding model using Biacore evaluation software. Goodness of fit was verified by U-value <25 and Chi-squared <10 as specified in the manufacturer's instructions.

2.6 Drug Loading and Release

Microparticles were solubilized in filtered diH_2O and SRL in dimethyl sulfoxide (DMSO). SRL was loaded in a 50:1 (drug:polymer) solution with a final solvent concentration of 50% DMSO and 50% diH_2O for 72 hours on a rotary shaker. Loading solutions were removed and particles were next mixed with release buffer (1x DPBS with 0.1% Tween80 which acts as a physiological buffer providing a hydrophobic sink [33, 40]) and incubated at 37°C on a rotary shaker. At pre-determined time points of 1 hour, 3 hours, and daily thereafter, the particles were centrifuged and release buffer was exchanged to monitor drug release and maintain sink conditions. SRL concentration was determined via a Synergy H1 Hybrid Multi-Mode Microplate Reader (BioTek Instruments, Inc., Winooski, VT) by measuring absorbance of the aliquots at 278 nm in a quartz microplate (Hellma, Plainview, NY) and

comparing to a SRL standard curve in release buffer. The release aliquots were stored at −20°C prior to further analysis.

2.7 Cell Proliferation

PT-K75 porcine mucosal fibroblasts (ATCC.org, Manassas, VA) were grown in Dulbecco's Modified Eagle's Medium (DMEM) supplemented with 10% fetal bovine serum (FBS) and 1% penicillin/streptomycin using standard culture methods at 37°C with 5% CO_2. Cells were plated at 6,000 cells per well in a 96 well tissue culture treated plate and allowed to adhere in media for 1.5 hours. Next, a fraction of SRL release aliquots or buffer control aliquots were added to the media and incubated for 24 hours. Aliquot treatments were 100 ul each, volume matched with drug only controls and diluted with 100 ul culture media. 10 μl of 0.15 mg/ml resazurin (Thermo Fisher Scientific), which is used to evaluate metabolic activity in the alamarBlue assay for quantifying fibroblast viability and proliferation [41], was added per treatment well. After incubation for an additional 20 hours, fluorescence at 530/590 excitation/emission was measured with a Synergy H1 Microplate Reader (BioTek Instruments, Inc., Winooski, VT) and fluorescent signals were normalized to buffer controls.

2.8 Cell Migration - Scratch Assay

Porcine mucosal fibroblast cells were plated at 25,000 cells per well in a 96 well plate in serum starvation media (only 0.5% fetal bovine serum) and incubated overnight. Plates were then scratched uniformly using a 200 μl sterile pipette tip and a custom guide, washed with serum starvation media, and treated with aliquots of SRL or release buffer for 24 hours with microscope images taken before and at the end of treatment. Aliquot treatments were 100 ul each, volume matched with drug only controls and diluted with 100 ul culture media. ImageJ analysis tools were used to quantify the scratch closure and the results show the average change in scratch width normalized to buffer only controls.

2.9 In Vitro Tissue Retention Analysis - Diffusion

Amino-β-CD MPs were synthesized by pre-mixing 6-amino-6-deoxy-β-cyclodextrin (0.5 wt %) with epichlorohydrin-crosslinked β-cyclodextrin prepolymer before synthesizing microparticles as stated in methods above. Alexa Fluor 647 (AF647) NHS-ester (Thermo Fisher Scientific) was mixed with amino-β-CD MPs in 0.1M sodium bicarbonate buffer (pH 8.3) according to manufacturer's instructions for conjugation. The particles were then washed five times in MilliQ water and dialyzed against buffer for three days to remove excess free dye molecules before use. Porcine tissue was acquired for secondary use from animals on protocols approved by the Case Western Reserve University Institutional Animal Care and Use Committee. Esophageal tissue was dissected post-mortem and bisected into 2 cm wide strips to expose the lumen. 20 μl of near-infrared fluorescent pCD-β-MPs in DPBS were then injected *ex vivo* into the esophageal submucosa using a 25G needle and syringe. Tissue samples were protected from light and incubated in excess DPBS to simulate diffusion from tissue. Although this does not fully recapitulate particle retention *in vivo*, it does give a preliminary estimate for particle retention after injection as the large size of the particles inhibits clearance via blood capillaries in healthy tissue [42–43]. Remaining fluorescence in tissue samples was measured at each time point using an IVIS Spectrum imaging system and quantified using spectral unmixing and region of interest

(ROI) selection tools (PerkinElmer, Waltham, MA). After 28 days, tissues were frozen in optimal cutting temperature (OCT) compound (Thermo Fisher Scientific), cryosectioned, and mounted on slides for confocal imaging using a Leica DMI4000 B TCS SPE confocal microscope (Leica Camera Inc., Allendale, NJ). A 405 nm laser with a PMT capturing 420−550 nm light was used to image the tissue autofluorescence while a 647 laser with a PMT capturing 670−750 nm light was used for imaging the AF647 conjugated fluorescent pCD-β-MPs.

2.10 Microparticle Persistence with Simulated Saliva Flow

To measure persistence of the polymer microparticles under flow conditions, esophageal tissue was dissected post-mortem and bisected into 2 cm wide strips to expose the lumen. 20 μl of near-infrared fluorescent pCD-β-MPs or Dex-MPs (conjugated to AF647 NHS-ester via same technique as pCD-β-MPs, but with amino-dextran (Thermo Fisher Scientific)) in DPBS were injected at an angle of 45° and depth of 5mm *ex vivo* into the esophageal submucosa using a 25G needle. To recapitulate *in vivo* washout and explore the potential of leakage from injection site, simulated saliva flow was introduced at 1 mL/min via syringe pump with artificial saliva (0.1 wt% albumin in prepared saline [44]) over the esophageal tissue lumen. Flow was stopped at the indicated volumes to measure remaining fluorescence in tissue samples with an IVIS Spectrum imaging system and quantified using spectral unmixing and region of interest (ROI) selection tools (PerkinElmer, Waltham, MA).

2.11 Statistical Analysis

Data are represented as the mean with standard deviation or standard error of the mean where specified. Statistics were calculated using GraphPad Prism 7 software (GraphPad Software, La Jolla, CA). Statistical significance was defined as $p < 0.05$ following statistical tests with further specifications noted in the figure captions.

3. Results

3.1 Affinity-based Delivery Predicted by Micromolar Affinity Between SRL and β-CD

Molecular docking was performed *in silico* to determine the strength of SRL interactions with potential hosts for affinity-based drug delivery. A set of common cyclodextrins were screened as host macromolecules and SRL was simulated as the ligand with binding energy minimizations simulated in Autodock Vina software (Figure 1A). The simulations indicated the strongest average affinity (lower K_D) for β-CD (22.51 μM) versus γ-CD (49.31 μM) or α-CD (103.52 μM). Dextran was simulated as a chemically similar control, but without a central cavity capable of forming an inclusion complex resulting in a much lower binding strength (1671.7 μM) comparable to previous studies [33, 45].

Additionally, all cyclodextrin and SRL complex affinity interactions were measured directly by SPR (Figure 1B). We have observed previous success for affinity-based drug delivery for affinity constants in the micromolar range [33]. Interactions between flowing SRL and surface-bound 6-amino-6-deoxy-β-CD demonstrated a K_D in the micromolar range via steady state affinity (81.24 μM) and Langmuir 1:1 kinetics (97.11 μM) models. Alternatively, flowing SRL interactions with surface-bound α-CD (510 μM) and γ-CD (146 μM) resulted in less

affinity binding, in agreement to the trend of the previous PyRx simulation results with slight differences due to estimations in the simulation. Reported K_D values were within the model confidence interval with Chi^2 values below 10% of the maximum SPR response [33]. Therefore, β-CD was chosen to maximize affinity-based delivery of SRL and dextran was used as a low-affinity control to determine the improvement in SRL delivery due to affinity interactions.

3.2 pCD-β-MP Delivery Increases the Amount and Timeframe of SRL Release

β-CD prepolymer lightly crosslinked with epichlorohydrin was further crosslinked with ethylene glycol diglycidyl ether using an inverse emulsion polymerization method to create insoluble microparticles with a high CD concentration for drug delivery [34]. Excess SRL was loaded at a 50:1 ratio of drug to polymer to maximize particle loading. After 72 hours, loading solution was removed and particles were suspended in release buffer in separate tubes with measurements taken at predetermined time points. The linear detection range was calculated to be from 125 to 1.9 μg/ml for SRL in release buffer. As expected pCD-β-MPs maintained a consistent daily release while non-affinity material, Dex-MPs demonstrated an initial burst release of 27 μg/ml SRL in the first hour followed by a drop in concentration to 8.8 μg/ml by day 3 (Figure 2A). The pCD-β-MPs not only provided a significantly longer delivery window but also released an average of 1314.9 μg SRL/mg polymer/day for the first 21 days of release which was twice the average daily amount released by the Dex-MPs.

Considering the cumulative release data (Figure 2B), the Dex-MPs released SRL more rapidly in the first four days, while the pCD-β-MPs exhibited higher cumulative delivery during later time points on days 16−23 of release. The pCD-β-MPs exhibited relatively little initial burst release in the first day (9% of total released) versus the 18.8% burst release from Dex-MPs. This trend was observed in previous studies to be associated with affinity interactions which reduce burst release while extending the drug delivery profile versus control non-affinity polymers [33].

Not only was the average daily amount and rate influenced by affinity, but the total amount of SRL released over the 30 day period was 1.5 times greater for the pCD-β-MPs. The pCD-β-MPs released an average of 36852 μg SRL per mg polymer while the Dex-MPs released 24406 μg SRL per mg polymer in solution (Figure 2C).

The loading efficiency was 73.7 ± 2.3% for pCD-β-MPs and 48.8±1.4% for Dex-MPs (Figure 2D). The higher drug loading efficiency of the pCD-β-MPs is likely due to affinity interactions and contributes to the greater amount of drug release observed from the pCD-β-MPs over time.

3.3 Released SRL Reduces Fibroblast Proliferation In Vitro

A fraction of release aliquots were applied to porcine PT-K75 mucosal fibroblasts *in vitro* to determine if SRL maintains bioactivity via reducing proliferation following delivery from polymer microparticles. Optimum incubation time and cell plating density were determined for the resazurin reduction assay to measure metabolic activity as a proxy for proliferation [41]. The volume matched SRL release aliquots from pCD-β-MPs and Dex-MP both maintained a bioactive effect in reducing cellular proliferation relative to buffer treated

controls (Figure 3A). The standard curve indicated that free drug alone had a similar effect to the released SRL (Figure 3B). The trend for early time points correlated with SRL release in the 10−30 μg/ml range corresponding to proliferation of ~60−70% relative to buffer control. The two polymers' release activity at days 21 and 28 gave similar results as expected for the similar release amounts at the indicated time points. Albeit released SRL maintained an anti-proliferative effect up to 28 days after the initial drug release study was began *in vitro*, indicating the potential for extended biological activity following long-term release *in vivo*.

3.4 Porcine Fibroblast Migration Inhibited by Released SRL

SRL bioactivity was also measured against cell migration. PT-K75 porcine fibroblast monolayers were scratched with a pipette tip and a fraction of SRL release aliquots were applied in serum starvation media [46]. Culture conditions and plating density were optimized prior to testing release aliquots (volume matched to controls) and images of the scratch assay setup are presented in Supplementary Figure S1. Day 1 and 7 aliquots of pCD-β-MPs released SRL completely inhibited PT-K75 cellular migration as compared to Dex-MP (Figure 4A). At day 21 and 28, both pCD-β-MPs and Dex-MP released SRL were capable of partially inhibiting migration as compared to the buffer treated controls. Similar activity was observed for free SRL drug alone (Figure 4B) with 10 μg/ml inhibiting migration by approximately 50%, which is comparable to the day 21 and day 28 release aliquots. These results corroborate the potential for pCD-β-MPs delivery of bioactive SRL to inhibit migration for up to 28 days post-loading.

3.5 Polymerized Particles Retain Their Size After 30 Day Incubation

Particle sizes were measured to ensure that pCD-β-MPs and Dex-MPs remained intact in physiological solution at 37°C over the four weeks required for wound healing resolution. Particles were imaged at 1 and 30 days post-incubation in release buffer (Figure 5A). Measured particle diameters and standard deviations at day 1 and day 30 were 14.68±5.28 μm and 13.81±4.31 μm for the pCD-β-MPs while the Dex-MP diameters were 23.87±8.97 μm and 23.16±9.31 μm, respectively (Figure 5B). Mean particle sizes were observed to remain constant over the 30 days of incubation in buffer with no indication of derivative products released in solution. As hypothesized the size of particles did not change; therefore results indicate that drug release from the synthesized particles was not due to particle degradation or erosion and that both polymer microparticles are able to maintain their size for extended time periods in physiological buffer.

3.6 In Vitro Tissue Retention of pCD-β-MPs

Our pCD particles not only extend the delivery window of SRL, but also improve localization of the released drug due to their limited degradation rate and macroscopic size. As a proof of concept test for particle retention in tissue, porcine esophageal tissue strips were injected *ex vivo* with near-infrared fluorescently labeled AF647-pCD-β-MPs and maintained in excess physiological buffer (Figure 6A). Fluorescence signal was measured longitudinally and it was observed that 16.7% of the initial signal remained after 28 days despite tissue degradation and less than ideal retention conditions in this mock scenario (Figure 6B). The half-life of retention was calculated to be 3.07±8.72 days by a one phase

decay model (R^2=0.8721). Confocal imaging of tissue slices confirmed that AF647-pCD-β-MPs were intact within tissue 28 days after injection and that the fluorescence signal was still co-localized with particles (Figure 6C). Contrastingly, after the injection of small molecule dye alone, similar in size to unbound SRL, only 4% of the initial amount remained after 28 days in buffer.

3.7 In Vitro Tissue Retention of Polymeric Microparticles with Simulated Saliva Flow

To further test the persistence of our polymer microparticles after injection in esophageal tissue, we have adapted other models of drug adhesion in the esophagus with simulated saliva flow [47–48]. Esophageal tissue strips were injected *ex vivo* and the initial signal of fluorescent particles was compared to the signal remaining after 1 ml and 10 ml of washout (Figure 7A). With a 25G needle, which is typically used for endoscopic procedures, we did not observe any significant leakage of either pCD-β-MPs or Dex-MPs from the injection site. Microparticle persistence was also similar between both polymer particles, indicating that 15−25 micron diameter particles have a potential for high retention in esophageal tissue under physiological flow conditions (Figure 7B).

4. Discussion

Our work demonstrated that inclusion of affinity components (Figure 1) in a polymer microparticle has the capacity to both increase the total amount of SRL loaded in the polymer and mediate the release rate of SRL to a more physiologically relevant profile (Figure 2). Because particles were synthesized with only CD and a low-molecular weight crosslinker we were able to achieve a high concentration of molecular “pockets” within the particles. It is hypothesized that the drug release profile in our work (Figure 2) was due to a multitude of affinity-based interactions occurring as drug diffused through the particle structure [45, 49]. Herein we show that affinity can be leveraged to increase drug loading of pCD systems but needs to be balanced to provide an appropriate context-dependent release rate [36]. For example, using a derivate cyclodextrin, such as methyl-β-CD which exhibits even greater affinity for SRL [50], may result in higher drug loading, but would further limit the release rate and effective release concentration of the system. The affinity-based delivery profile achieved in our work appears to balance sufficient loading with release of biologically active SRL for the four weeks required for stable wound healing following ESD (Figures 3 and 4) [20, 37]. The pCD-β-MPs retained their physical size during the incubation period (Figure 5) indicating that drug release was mediated mainly by diffusion and affinity-based mechanisms rather than degradation or erosion [26, 51]. Other techniques such as molecular imprinting could be utilized to further improve cyclodextrin polymer drug loading [52]. Moreover, as the polymer persists at the injection site (Figure 6, 7), there is a potential for a booster effect in which the particles can be re-loaded with a local drug dose if needed [53]. This reloading can extend the release profile and local concentration which may aid in dealing with refractory strictures [54].

Our drug/device platform fills a gap in the field as other materials and devices such as drug eluting stents, nanoparticles, and thin films have been tested for SRL delivery in other disease contexts, but have not been validated for esophageal drug delivery. Using

nanoemulsion techniques, acetylated β-CD nanoparticles 250 nm in diameter were found capable of SRL delivery for 20 days *in vitro*, yet neither *in vivo* retention nor direct anti-fibrotic activity was reported [55]. SRL eluting cardiovascular stents were crafted to deliver 14–28 days of continuous release, but the initial burst release is high with the following continuous release at a much lower concentration [56]. Interestingly, insoluble pellets of SRL trapped in microporous polycaprolactone thin films provided the longest delivery of up to 16 weeks of SRL release, but this results in a daily concentration which may be below the effective dose and the application of such a film to the esophageal wall should be tested in future studies [57].

We test injected our polymer microparticle suspensions through a 25G endoscopic needle. This is critical for translational potential using commercially available endoscopic needles. Additionally, while no adverse response has been observed in animals implanted with pCD disks and microparticles [34, 58], exact immune system interactions still need to be determined, especially in an inflammatory context. There have been very few previous attempts at particle injections within the esophagus. Previous studies have focused on anti-cancer drug delivery or tissue bulking [59–60], which leaves many unanswered questions to be explored in future studies of esophageal drug delivery. Injectability of microspheres in the esophagus and localization is hypothesized to be important as to inhibit fibroblast migration from the muscle layer yet allow for epithelial migration/proliferation and wound healing to occur laterally from the periphery of dissected tissue [61]. Local delivery of SRL to the esophagus post-ESD is expected to promote wound healing by preventing excessive fibroblast proliferation similar to previous results with mitomycin C without the cytotoxic drawbacks [20, 62]. However, SRL may potentially lengthen the time to resolve healing *in vivo* due to anti-inflammatory and other reported effects, yet this may be a dose balancing issue [63–64]. Alternatively, other molecules promoting wound healing may be co-delivered, such as trefoil peptides, growth factors, polyamines, and more [65–66] which could promote the healing of the epithelium and may be applied via a different set of drug-loaded pCD-MP injections for a greater combined effect than anti-fibrotic therapy alone.

5. Conclusions:

Cyclodextrin pre-polymers were formulated into microparticles capable of sustained SRL delivery over the course of four weeks. The released SRL was confirmed to be bioactive against fibrotic processes in assays against porcine fibroblast proliferation and migration *in vitro*. pCD-β-MPs retained their size after injection and were localized in esophageal tissue 28 days after injection and incubation *ex vivo*. This combination of an injectable microparticle platform which remains localized in tissue interstitium and affinity-based drug delivery for continuous long-term release regardless of physical properties exhibits potential for preventing esophageal stricture.

Supplementary Material

Refer to Web version on PubMed Central for supplementary material.

Acknowledgments

The authors would like to acknowledge support from R03CA204890-01A1 and T32DK083251-09 (NAR) and from an NIH Research Facilities Construction Grant (C06 RR12463-01).

References:

1. Noone AM HN, Krapcho M, Miller D, Brest A, Yu M, Ruhl J, Tatalovich Z, Mariotto A, Lewis DR, Chen HS, Feuer EJ, Cronin KA (eds), SEER Cancer Statistics Review. National Cancer Institute 2017.
2. Moinova HR; LaFramboise T; Lutterbaugh JD; Chandar AK; Dumot J; Faulx A; Brock W; De la Cruz Cabrera O; Guda K; Barnholtz-Sloan JS; Iyer PG; Canto MI; Wang JS; Shaheen NJ; Thota PN; Willis JE; Chak A; Markowitz SD, Identifying DNA methylation biomarkers for non-endoscopic detection of Barrett's esophagus. Science Translational Medicine 2018, 10 (424).
3. Mizuta H; Nishimori I; Kuratani Y; Higashidani Y; Kohsaki T; Onishi S, Predictive factors for esophageal stenosis after endoscopic submucosal dissection for superficial esophageal cancer. Diseases of the Esophagus 2009, 22 (7), 626–631. [PubMed: 19302207]
4. Lewis JJ; Rubenstein JH; Singal AG; Elmunzer BJ; Kwon RS; Piraka CR, Factors associated with esophageal stricture formation after endoscopic mucosal resection for neoplastic Barrett's esophagus. Gastrointestinal endoscopy 2011, 74 (4), 753–760. [PubMed: 21820109]
5. Kim GH; Jee SR; Jang JY; Shin SK; Choi KD; Lee JH; Kim SG; Sung JK; Choi SC; Jeon SW; Jang BI; Huh KC; Chang DK; Jung S-A; Keum B; Cho JW; Choi IJ; Jung H-Y; Korean ESDSG, Stricture Occurring after Endoscopic Submucosal Dissection for Esophageal and Gastric Tumors. Clinical Endoscopy 2014, 47 (6), 516–522. [PubMed: 25505717]
6. Jain S; Dhingra S, Pathology of esophageal cancer and Barrett's esophagus. Annals of Cardiothoracic Surgery 2017, 6 (2), 99–109. [PubMed: 28446998]
7. Deprez PH, Barrett's esophagus: The advocacy for ESD. Endoscopy International Open 2016, 4 (6), E722–E724. [PubMed: 27556084]
8. Shimura T; Sasaki M; Kataoka H; Tanida S; Oshima T; Ogasawara N; Wada T; Kubota E; Yamada T; Mori Y; Fujita F; Nakao H; Ohara H; Inukai M; Kasugai K; Joh T, Advantages of endoscopic submucosal dissection over conventional endoscopic mucosal resection. Journal of gastroenterology and hepatology 2007, 22 (6), 821–6. [PubMed: 17565635]
9. Das A; Singh V; Fleischer DE; Sharma VK, A comparison of endoscopic treatment and surgery in early esophageal cancer: an analysis of surveillance epidemiology and end results data. The American journal of gastroenterology 2008, 103 (6), 1340–5. [PubMed: 18510606]
10. Takahashi H; Arimura Y; Masao H; Okahara S; Tanuma T; Kodaira J; Kagaya H; Shimizu Y; Hokari K; Tsukagoshi H; Shinomura Y; Fujita M, Endoscopic submucosal dissection is superior to conventional endoscopic resection as a curative treatment for early squamous cell carcinoma of the esophagus (with video). Gastrointest Endosc 2010, 72 (2), 255–64, 264.e1–2. [PubMed: 20541198]
11. Joo DC; Kim GH; Park DY; Jhi JH; Song GA, Long-Term Outcome after Endoscopic Submucosal Dissection in Patients with Superficial Esophageal Squamous Cell Carcinoma: A Single-Center Study. Gut and Liver 2014, 8 (6), 612–8. [PubMed: 25368748]
12. Nonaka K; Miyazawa M; Ban S; Aikawa M; Akimoto N; Koyama I; Kita H, Different healing process of esophageal large mucosal defects by endoscopic mucosal dissection between with and without steroid injection in an animal model. BMC Gastroenterology 2013, 13 (1), 72. [PubMed: 23617935]
13. Katada C; Muto M; Manabe T; Boku N; Ohtsu A; Yoshida S, Esophageal stenosis after endoscopic mucosal resection of superficial esophageal lesions. Gastrointestinal Endoscopy 2003, 57 (2), 165–169. [PubMed: 12556777]
14. Hanaoka N; Ishihara R; Takeuchi Y; Uedo N; Higashino K; Ohta T; Kanzaki H; Hanafusa M; Nagai K; Matsui F; Iishi H; Tatsuta M; Ito Y, Intralesional steroid injection to prevent stricture after endoscopic submucosal dissection for esophageal cancer: a controlled prospective study. Endoscopy 2012, 44 (11), 1007–11. [PubMed: 22930171]

15. Hashimoto S; Kobayashi M; Takeuchi M; Sato Y; Narisawa R; Aoyagi Y, The efficacy of endoscopic triamcinolone injection for the prevention of esophageal stricture after endoscopic submucosal dissection. Gastrointest Endosc 2011, 74 (6), 1389–93. [PubMed: 22136782]
16. Kobayashi S; Kanai N; Ohki T; Takagi R; Yamaguchi N; Isomoto H; Kasai Y; Hosoi T; Nakao K; Eguchi S; Yamamoto M; Yamato M; Okano T, Prevention of esophageal strictures after endoscopic submucosal dissection. World Journal of Gastroenterology : WJG 2014, 20 (41), 15098–15109. [PubMed: 25386058]
17. Abe S; Iyer PG; Oda I; Kanai N; Saito Y, Approaches for stricture prevention after esophageal endoscopic resection. Gastrointestinal Endoscopy 2017, 86 (5), 779–791. [PubMed: 28713066]
18. Chai N-L; Feng J; Li L-S; Liu S-Z; Du C; Zhang Q; Linghu E-Q, Effect of polyglycolic acid sheet plus esophageal stent placement in preventing esophageal stricture after endoscopic submucosal dissection in patients with early-stage esophageal cancer: A randomized, controlled trial. World Journal of Gastroenterology 2018, 24 (9), 1046–1055. [PubMed: 29531468]
19. Wang W; Ma Z, Steroid Administration is Effective to Prevent Strictures After Endoscopic Esophageal Submucosal Dissection: A Network Meta-Analysis. Medicine 2015, 94 (39), e1664. [PubMed: 26426665]
20. Wu Y; Schomisch SJ; Cipriano C; Chak A; Lash RH; Ponsky JL; Marks JM, Preliminary results of antiscarring therapy in the prevention of postendoscopic esophageal mucosectomy strictures. Surgical endoscopy 2014, 28 (2), 447–455. [PubMed: 24100858]
21. Yan Z.-c.; Bai Y.-j.; Tian Z; Hu H.-y.; You X.-h.; Lin J.-x.; Liu S.-r.; Zhuo Y.-h.; Luo R.-j., Anti-proliferation effects of Sirolimus sustained delivery film in rabbit glaucoma filtration surgery. Molecular Vision 2011, 17, 2495–2506. [PubMed: 21976960]
22. Moses JW; Leon MB; Popma JJ; Fitzgerald PJ; Holmes DR; O'Shaughnessy C; Caputo RP; Kereiakes DJ; Williams DO; Teirstein PS; Jaeger JL; Kuntz RE, Sirolimus-Eluting Stents versus Standard Stents in Patients with Stenosis in a Native Coronary Artery. New England Journal of Medicine 2003, 349 (14), 1315–1323. [PubMed: 14523139]
23. Mahalati K; Kahan BD, Clinical pharmacokinetics of sirolimus. Clinical pharmacokinetics 2001, 40 (8), 573–85. [PubMed: 11523724]
24. MacDonald A; Scarola J; Burke JT; Zimmerman JJ, Clinical pharmacokinetics and therapeutic drug monitoring of sirolimus. Clinical therapeutics 2000, 22 Suppl B, B101–121. [PubMed: 10823378]
25. Wang NX; von Recum HA, Affinity-Based Drug Delivery. Macromolecular Bioscience 2010, 11 (3), 321–332. [PubMed: 21108454]
26. Halpern JM; Gormley CA; Keech M; von Recum HA, Thermomechanical Properties, Antibiotic Release, and Bioactivity of a Sterilized Cyclodextrin Drug Delivery System. Journal of materials chemistry. B, Materials for biology and medicine 2014, 2 (18), 2764–2772. [PubMed: 24949201]
27. Fu AS; Thatiparti TR; Saidel GM; von Recum HA, Experimental Studies and Modeling of Drug Release from a Tunable Affinity-Based Drug Delivery Platform. Annals of Biomedical Engineering 2011, 39 (9), 2466–2475. [PubMed: 21678091]
28. Haley RM; von Recum HA, Localized and targeted delivery of NSAIDs for treatment of inflammation: A review. Experimental Biology and Medicine 2018, 1535370218787770.
29. Cyphert EL; von Recum HA, Emerging technologies for long-term antimicrobial device coatings: advantages and limitations. Experimental Biology and Medicine 2017, 242 (8), 788–798. [PubMed: 28110543]
30. Halpern JM; von Recum HA, Affinity-based delivery systems. In Biomaterials and Regenerative Medicine, Ma PX, Ed. Cambridge University Press: Cambridge, 2014; pp 419–430.
31. Rivera-Delgado E; Nam JK; von Recum HA, Localized Affinity-Based Delivery of Prinomastat for Cancer Treatment. ACS Biomaterials Science & Engineering 2017, 3 (3), 238–242. [PubMed: 33465922]
32. Thatiparti TR; von Recum HA, Cyclodextrin Complexation for Affinity-Based Antibiotic Delivery. Macromolecular Bioscience 2009, 10 (1), 82–90.
33. Rivera-Delgado E; von Recum HA, Using Affinity To Provide Long-Term Delivery of Antiangiogenic Drugs in Cancer Therapy. Molecular Pharmaceutics 2017, 14 (3), 899–907. [PubMed: 28128564]

34. Grafmiller KT; Zuckerman ST; Petro C; Liu L; von Recum HA; Rosen MJ; Korley JN, Antibiotic-releasing microspheres prevent mesh infection in vivo. Journal of Surgical Research 2016, 206 (1), 41–47. [PubMed: 27916373]
35. Thatiparti TR; Shoffstall AJ; von Recum HA, Cyclodextrin-based device coatings for affinity-based release of antibiotics. Biomaterials 2010, 31 (8), 2335–47. [PubMed: 20022369]
36. Edgardo R-D; Zhina S; Nick XW; Jonathan K; Sapna S; Michael K; Chris F; Adonis ZH; Horst A. v. R., Local release from affinity-based polymers increases urethral concentration of the stem cell chemokine CCL7 in rats. Biomedical Materials 2016, 11 (2), 025022. [PubMed: 27097800]
37. Honda M; Nakamura T; Hori Y; Shionoya Y; Nakada A; Sato T; Yamamoto K; Kobayashi T; Shimada H; Kida N; Hashimoto A; Hashimoto Y, Process of healing of mucosal defects in the esophagus after endoscopic mucosal resection: histological evaluation in a dog model. Endoscopy 2010, 42 (12), 1092–1095. [PubMed: 21038294]
38. Trott O; Olson AJ, AutoDock Vina: improving the speed and accuracy of docking with a new scoring function, efficient optimization, and multithreading. Journal of computational chemistry 2010, 31 (2), 455–461. [PubMed: 19499576]
39. Dallakyan S; Olson AJ, Small-molecule library screening by docking with PyRx. Methods in molecular biology (Clifton, N.J.) 2015, 1263, 243–50.
40. Jhunjhunwala S; Balmert SC; Raimondi G; Dons E; Nichols EE; Thomson AW; Little SR, Controlled Release Formulations of IL-2, TGF-β1 and Rapamycin for the Induction of Regulatory T Cells. Journal of controlled release : official journal of the Controlled Release Society 2012, 159 (1), 78–84. [PubMed: 22285546]
41. Voytik-Harbin SL; Brightman AO; Waisner B; Lamar CH; Badylak SF, Application and evaluation of the alamarBlue assay for cell growth and survival of fibroblasts. In vitro cellular & developmental biology. Animal 1998, 34 (3), 239–46. [PubMed: 9557942]
42. Rohner NA; Thomas SN, Melanoma growth effects on molecular clearance from tumors and biodistribution into systemic tissues versus draining lymph nodes. J Control Release 2016, 223, 99–108. [PubMed: 26721446]
43. Rohner NA; Thomas SN, Flexible Macromolecule versus Rigid Particle Retention in the Injected Skin and Accumulation in Draining Lymph Nodes Are Differentially Influenced by Hydrodynamic Size. ACS Biomater Sci Eng 2017, 3 (2), 153–159. [PubMed: 29888321]
44. Amal ASS; Hussain S; Amin Jalaluddin M; Amal A, Preparation of Artificial Saliva Formulation 2015.
45. Rivera-Delgado E; Djuhadi A; Danda C; Kenyon J; Maia J; Caplan AI; von Recum HA, Injectable liquid polymers extend the delivery of corticosteroids for the treatment of osteoarthritis. Journal of Controlled Release 2018, 284, 112–121. [PubMed: 29906555]
46. Rodriguez LG; Wu X; Guan JL, Wound-healing assay. Methods in molecular biology (Clifton, N.J.) 2005, 294, 23–9.
47. Di Simone MP; Baldi F; Vasina V; Scorrano F; Bacci ML; Ferrieri A; Poggioli G, Barrier effect of Esoxx(®) on esophageal mucosal damage: experimental study on ex-vivo swine model. Clinical and experimental gastroenterology 2012, 5, 103–107. [PubMed: 22767997]
48. Richardson JC; Dettmar PW; Hampson FC; Melia CD, Oesophageal bioadhesion of sodium alginate suspensions 2. Suspension behaviour on oesophageal mucosa. European journal of pharmaceutical sciences : official journal of the European Federation for Pharmaceutical Sciences 2005, 24 (1), 107–14. [PubMed: 15626584]
49. von Recum HA Therapeutic agent delivery system and method 10,045,937, 2010.
50. Abdur Rouf M; Vural I; Bilensoy E; Hincal A; Erol DD, Rapamycin-cyclodextrin complexation: improved solubility and dissolution rate. Journal of Inclusion Phenomena and Macrocyclic Chemistry 2011, 70 (1), 167–175.
51. Fu A. S. v. R., Horst A, Affinity-Based Drug Delivery. In Engineering Polymer Systems for Improved Drug Delivery, 2014.
52. Juric D; Rohner NA; von Recum HA, Molecular Imprinting of Cyclodextrin Supramolecular Hydrogels Improves Drug Loading and Delivery. Macromolecular Bioscience 2019, 19 (1), 1800246.

53. Cyphert EL; Learn GD; Hurley SK; Lu C.-y.; von Recum HA, Bone Cements: An Additive to PMMA Bone Cement Enables Postimplantation Drug Refilling, Broadens Range of Compatible Antibiotics, and Prolongs Antimicrobial Therapy (Adv. Healthcare Mater. 21/2018). Advanced Healthcare Materials 2018, 7 (21), 1870080.
54. Cyphert EL; Zuckerman ST; Korley JN; von Recum HA, Affinity interactions drive post-implantation drug filling, even in the presence of bacterial biofilm. Acta Biomaterialia 2017, 57, 95–102. [PubMed: 28414173]
55. Dou Y; Guo J; Chen Y; Han S; Xu X; Shi Q; Jia Y; Liu Y; Deng Y; Wang R; Li X; Zhang J, Sustained delivery by a cyclodextrin material-based nanocarrier potentiates antiatherosclerotic activity of rapamycin via selectively inhibiting mTORC1 in mice. Journal of Controlled Release 2016, 235 (C), 48–62. [PubMed: 27235978]
56. Raval A; Parikh J; Engineer C, Mechanism and in Vitro Release Kinetic Study of Sirolimus from a Biodegradable Polymeric Matrix Coated Cardiovascular Stent. Industrial & Engineering Chemistry Research 2011, 50 (16), 9539–9549.
57. Lance KD; Good SD; Mendes TS; Ishikiriyama M; Chew P; Estes LS; Yamada K; Mudumba S; Bhisitkul RB; Desai TA, In Vitro and In Vivo Sustained Zero-Order Delivery of Rapamycin (Sirolimus) From a Biodegradable Intraocular Device. Investigative ophthalmology & visual science 2015, 56 (12), 7331–7337. [PubMed: 26559479]
58. Blatnik JA; Thatiparti TR; Krpata DM; Zuckerman ST; Rosen MJ; von Recum HA, Infection prevention using affinity polymer-coated, synthetic meshes in a pig hernia model. Journal of Surgical Research 2017, 219, 5–10. [PubMed: 29078909]
59. Hagiwara A; Takahashi T; Kitamura K; Sakakura C; Shirasu M; Ohgaki M; Imanishi T; Yamasaki J, Endoscopic local injection of a new drug delivery formulation, anticancer drug bound to carbon particles, for digestive cancers: pilot study. Journal of gastroenterology 1997, 32 (2), 141–7. [PubMed: 9085159]
60. Kamler JP; Lemperle G; Lemperle S; Lehman GA, Endoscopic lower esophageal sphincter bulking for the treatment of GERD: safety evaluation of injectable polymethylmethacrylate microspheres in miniature swine. Gastrointest Endosc 2010, 72 (2), 337–42. [PubMed: 20541193]
61. Barret M; Beye B; Leblanc S; Beuvon F; Chaussade S; Batteux F; Prat F, Systematic review: the prevention of oesophageal stricture after endoscopic resection. Alimentary pharmacology & therapeutics 2015, 42 (1), 20–39. [PubMed: 25982288]
62. Berger M; Ure B; Lacher M, Mitomycin C in the therapy of recurrent esophageal strictures: hype or hope? European journal of pediatric surgery : official journal of Austrian Association of Pediatric Surgery … [et al] = Zeitschrift fur Kinderchirurgie 2012, 22 (2), 109–16.
63. Schaffer M; Schier R; Napirei M; Michalski S; Traska T; Viebahn R, Sirolimus impairs wound healing. Langenbeck's archives of surgery 2007, 392 (3), 297–303.
64. Knight RJ; Villa M; Laskey R; Benavides C; Schoenberg L; Welsh M; Kerman RH; Podder H; Van Buren CT; Katz SM; Kahan BD, Risk factors for impaired wound healing in sirolimus-treated renal transplant recipients. Clinical transplantation 2007, 21 (4), 460–5. [PubMed: 17645704]
65. Sturm A; Dignass AU, Epithelial restitution and wound healing in inflammatory bowel disease. World Journal of Gastroenterology : WJG 2008, 14 (3), 348–353. [PubMed: 18200658]
66. Iizuka M; Konno S, Wound healing of intestinal epithelial cells. World Journal of Gastroenterology : WJG 2011, 17 (17), 2161–2171. [PubMed: 21633524]

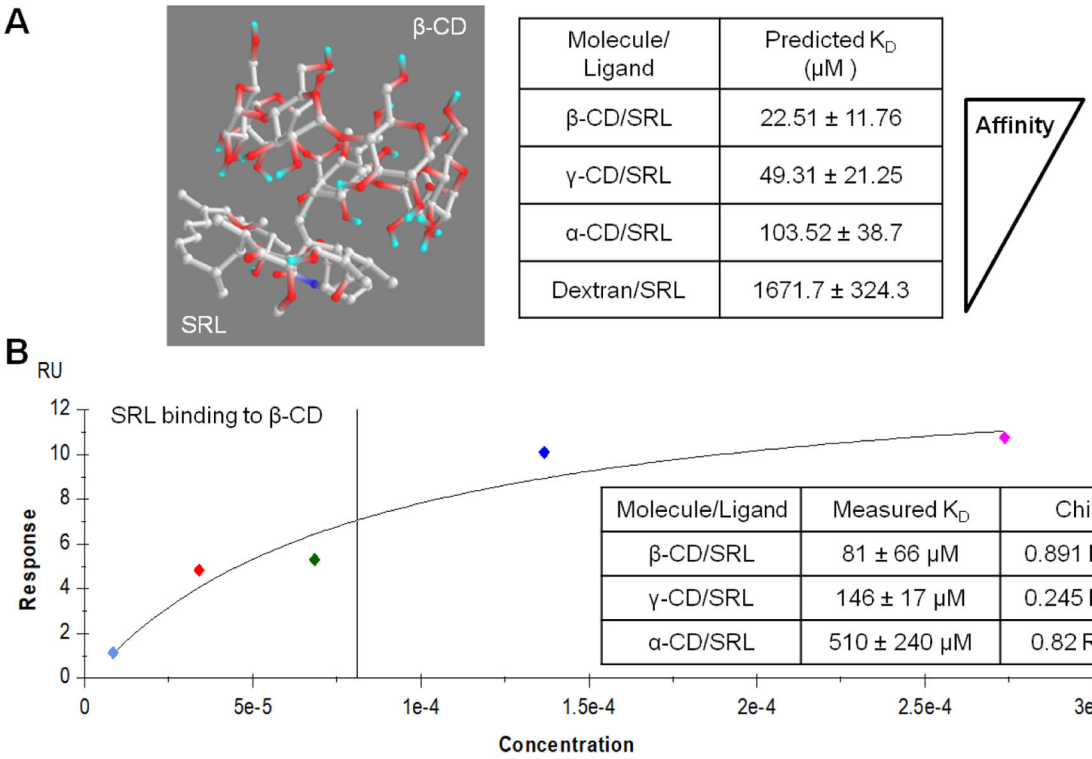

Figure 1.

PyRx simulated SRL complexation with cyclodextrin monomers and predicted binding affinity with standard deviation derived from different possible conformations (A). Experimental determination of SRL and β-CD affinity measured by SPR indicates lowest affinity (B).

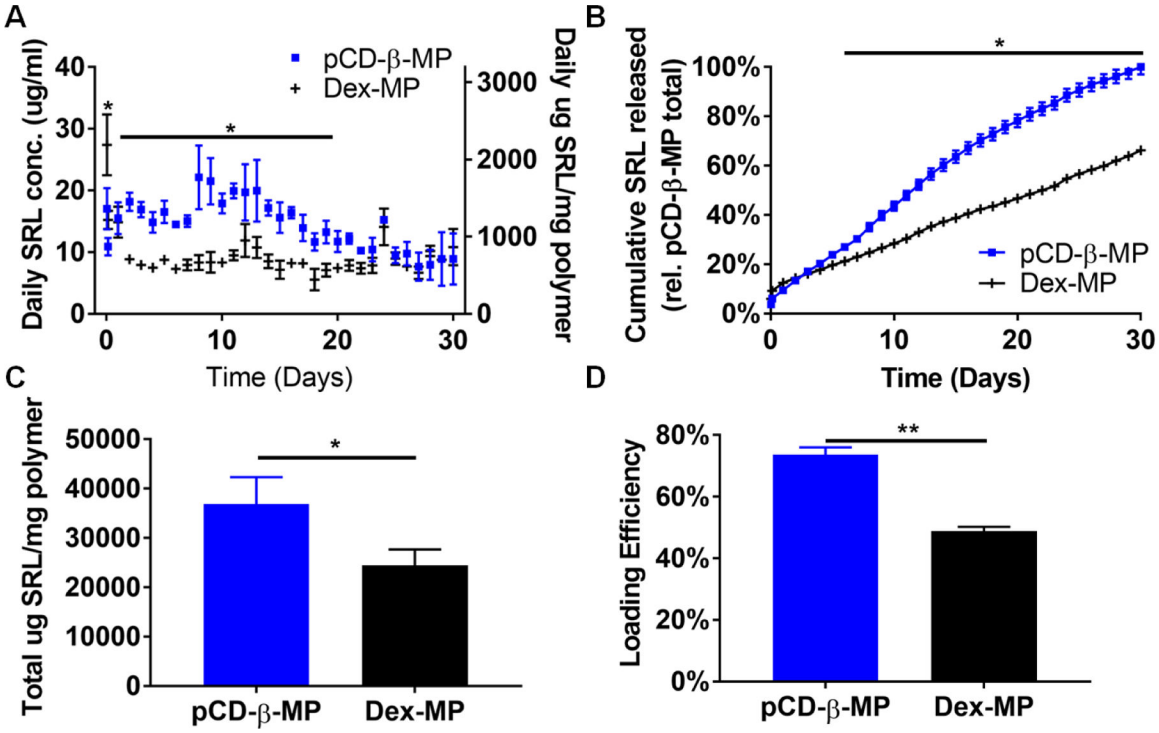

Figure 2.

Released SRL in buffer was measured daily from pCD-β-MP and Dex-MP (A, left) and normalized to the amount of total polymeric particles weighed before loading (A, right). The normalized daily cumulative depicts the rate of SRL release (B). Total SRL released was calculated from daily release data (C) and loading efficiency was determined by mass released divided by mass of drug initially added to samples (D). n=3 separate samples per group; error bars represent standard deviation; * indicates $p < 0.05$ by two-way ANOVA with Bonferroni test post-hoc Days 2−19 for (A), Days 6−30 for (B) or by Student's t-test for (C, D).

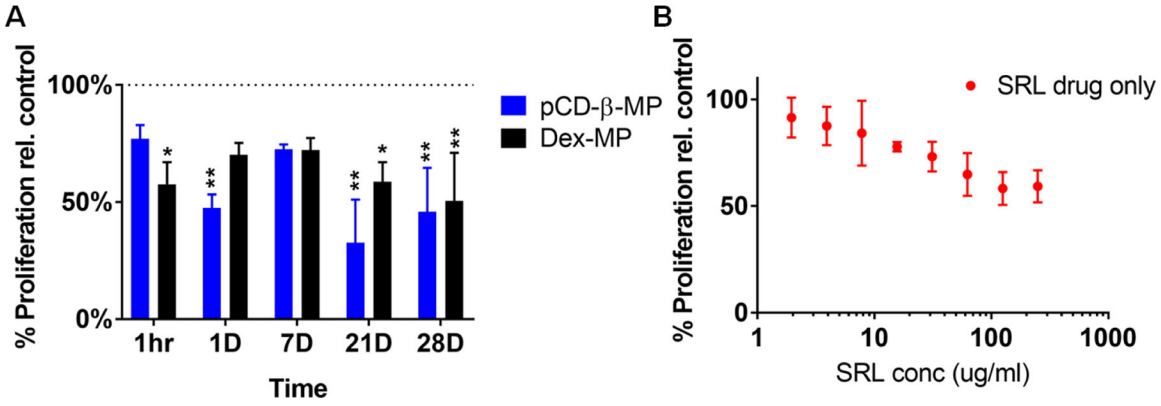

Figure 3.

Proliferation of pig fibroblast cells (PT-K75) was measured by Alamarblue assay after 44 hour incubation with daily SRL release aliquots from pCD-β-MP and Dex-MP (A) and standard curve validating the drug's activity alone (B). n=3 separate wells per group; * indicates $p < 0.05$, ** $p < 0.01$ by two-way ANOVA with Bonferroni test post-hoc versus 100% buffer controls; error bars represent standard error of the mean.

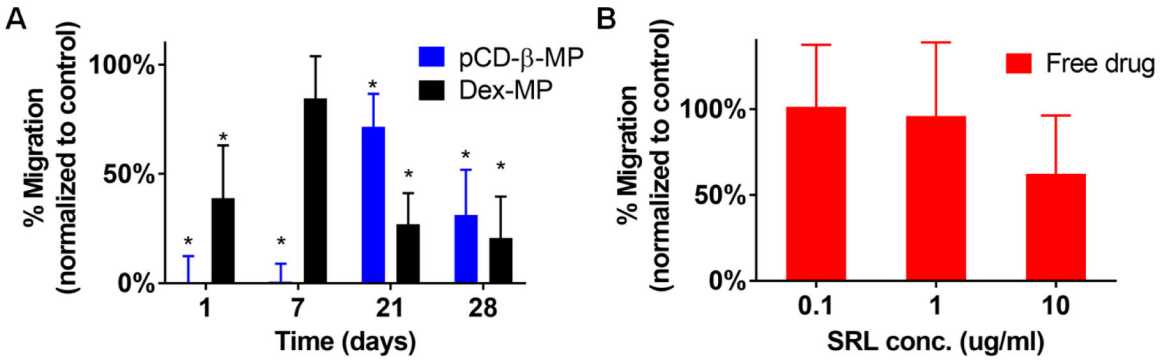

Figure 4.

PT-K75 porcine mucosal fibroblast migration into a scratched area after 24hr incubation with SRL aliquots from pCD-β-MP and Dex-MP in serum starvation media from indicated release times (A) and free drug applied at pre-determined concentrations for control (B). n=9 measurements per group; * indicates $p < 0.05$ by t-test versus controls incubated with buffer alone; error bars represent standard error of the mean.

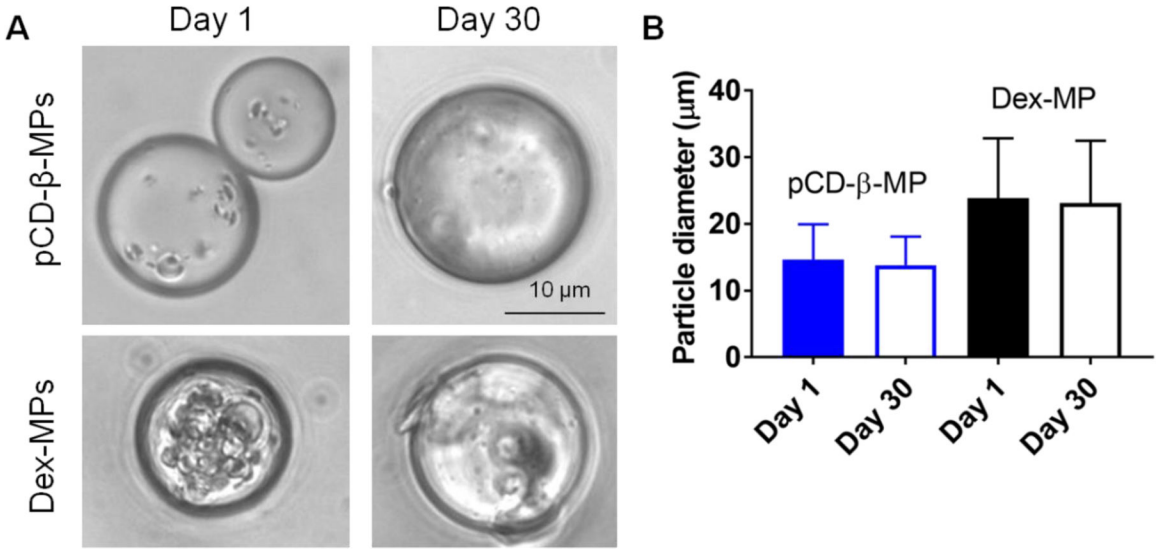

Figure 5.

Representative images of synthesized pCD-β-MP and dextran microparticles following 1 and 30 days incubation in physiological release buffer at 37°C (A). Particle diameters were calculated with ImageJ and presented as mean with standard deviation (B). n≥150 particles were measured per group; day 1 vs. day 30 by one-way ANOVA and Bonferroni test post-hoc were not significant as expected for pCD-β-MP (p=0.866) or Dex-MP (p=0.714).

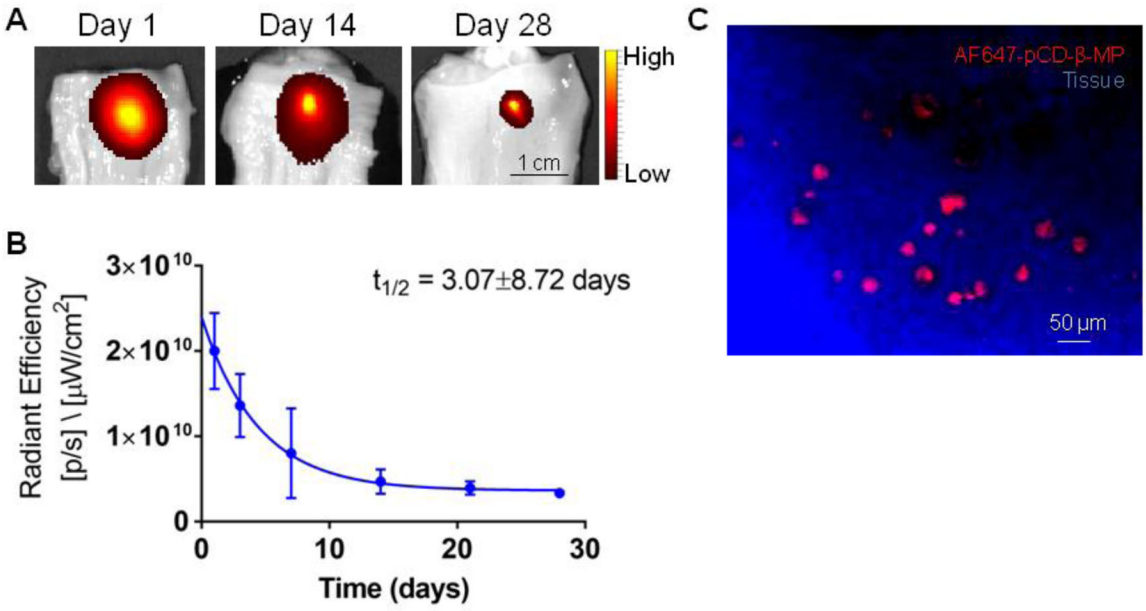

Figure 6.

Fluorescently conjugated pCD-β-MP were injected in excised esophageal tissue and incubated in DPBS solution with the remaining signal imaged at the indicated incubation times by IVIS (A) and quantified over time (B). Esophageal tissue was sectioned and imaged via confocal microscope to reveal fluorescently conjugated AF647-pCD-β-MPs remaining in tissue after 28 days incubation in buffer (C). n=2 replicates per time point.

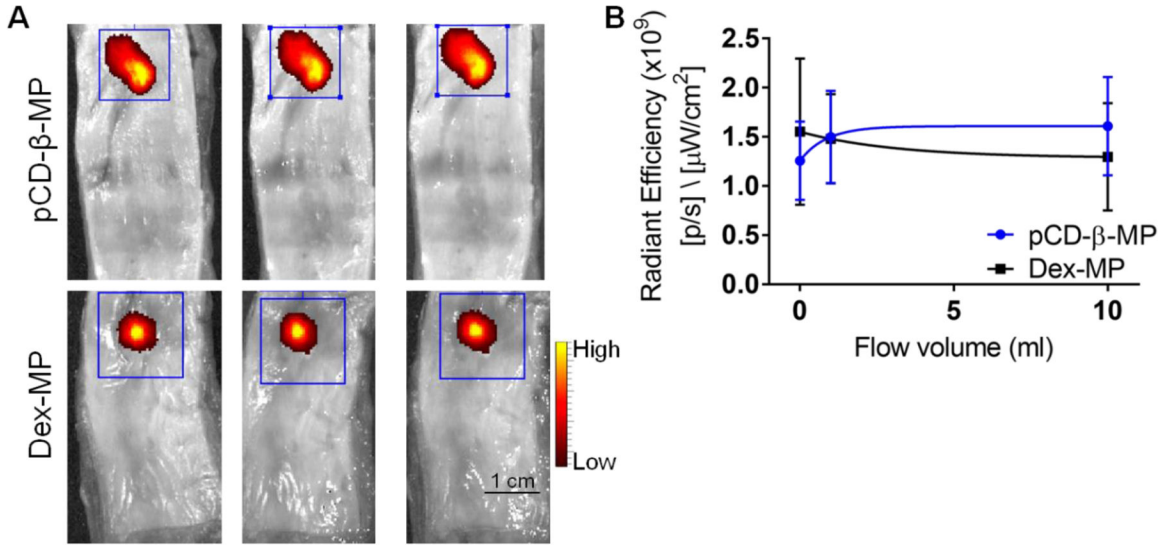

Figure 7.

Local persistence was tested after injection of both fluorescently labeled polymer microparticles in separate esophageal tissue samples (A) and exposed to simulated saliva flow conditions with remaining particles measured by fluorescence signal using IVIS (B). No significant particle leakage was observed from the injection site after flow. No significant differences were measured between the polymer microparticle types. n=3 replicates per time point; error bars represent standard error of the mean.